A Study on Shear Resisting Mechanism of RC Columns Strengthened with Carbon Fiber Sheets

Gabriel Sirbu*, Tamon Ueda**, Yoshio Kakuta***

*PhD candidate, Graduate School of Eng., Hokkaido University, Kita-ku, Sapporo, 060-8628
**Dr. of Eng., Associate Professor, Graduate School of Eng., Hokkaido University, Kita-ku, Sapporo, 060-8628
***Dr. of Eng., Professor, Graduate School of Eng., Hokkaido University, Kita-ku, Sapporo, 060-8628

This paper presents the results of FEM analysis of concrete column strengthened with carbon fiber sheet (CFS), where sheet and interface-bond element developed by the authors are used. The FEM analysis can predict ultimate loads as well as failure modes of tested specimens. The FEM results indicate that shear force carried by concrete decreases with increase in CFS amount, however shear force carried by CFS increases, which increases the shear capacity. It was found from the FEM analysis that the model for shear capacity of unstrengthened beam can be applied to cases of reinforced concrete elements strengthened with CFS by introducing equivalent stiffness of shear reinforcement.

Key Words: CFS, FEM, Shear, Strengthening

1. Introduction

Because of their high strength and their easiness in application the Fiber Reinforced Plastics (FRP) have been increasingly used in the process of strengthening in the recent years. The lack of knowledge of the shear resisting mechanism of the strengthened Reinforced Concrete (RC) members leads sometimes to rough approximations of the increase in strength and consequently to unnecessary costs.

The difference between the mechanical properties of the steel reinforcement (yielding material) used as shear reinforcement and FRP (non-yielding material) used in the strengthening of RC columns creates difficulties in the application of the known models for shear resisting capacity. Therefore, Sato et al. proposed a new model that can be applied to cases where tensile and shear reinforcements are either steel or FRP [1), 2), 3)]. However, this model cannot be applied directly to cases where steel and FRP are used together as either tensile or shear reinforcement and where FRP that is externally bonded to concrete is used as reinforcement.

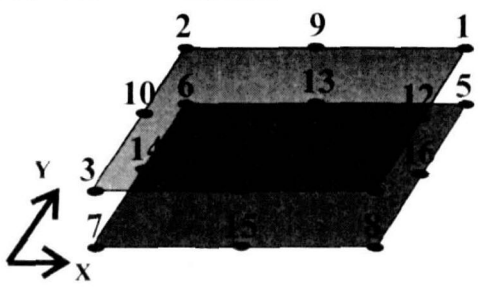

Fig. 1 Elements used in FEM analysis

In this study, unidirectional Carbon Fiber Sheet (CFS) impregnated and bonded with epoxy resin is used as strengthening material. Finite element analysis that is equipped with elements for FRP sheet and its interface-bonding layer, developed by the author[5)], was conducted. Based on the results of the FEM analysis, a modified model to predict shear capacity of columns strengthened with CFS was presented.

2. Development and validation of FEM program

The program used by the authors in this study is based on the FEM program, WCOMR, developed originally by Okamura and Maekawa[4)]. Sirbu et al.[5)] presents the modification of the original program and the implementation of newly developed elements for CFS and interface-bonding layer, which are used in this study. The modified program may be applied for the analysis of a cantilever beam or a column subjected to lateral forces, in which the FRP material is used as transverse reinforcement and is applied on the lateral surfaces of the member. In this case the FRP material is applied on the surface that is visible in the plane of analysis. The advantage of this method is that the analysis remains two-dimensional. Since it is considered that the stress and deformation in the third dimension have a very small influence on the shear capacity, a two-dimensional analysis gives reasonable results. The RC and CFS elements are modelled using 8 nodes isoparametric elements. Figure 1 shows the way in which the CFS and the RC elements are used in this analysis. The nodes 5, 6, 7, 8, 13,14, 15 and 16 denote the RC element. The nodes 1, 2, 3, 4, 9, 10, 11, 12 denote the CFS element.

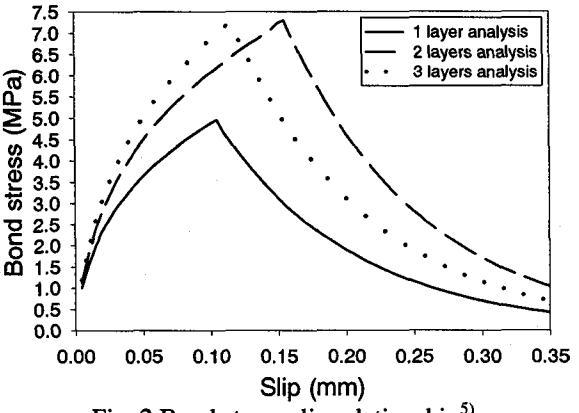

Fig. 2 Bond stress-slip relationship[5)]

The interface layer is defined using all the 16 nodes from the CFS and RC. The stress-strain relationship for the CFS along the fiber direction is considered linear elastic until failure. Figure 2 presents the bond stress-slip relationship for the interface-bonding layer. The maximum bond stress and the corresponding slip depend on the CFS stiffness and concrete strength.

The bond stress-slip relationship can be expressed in a simplified manner as follows[5)]:

$$\tau = \frac{\tau_{max}}{s_0} G_0 D^* s \tag{1}$$

before maximum bond stress and

$$\tau = \tau_{max} \exp[-10(s - s_0)] \tag{2}$$

after maximum bond stress, where

$$s_0 = 0.8 \times 10^{-12} (tE_{CFS})^{2.4} f_c'^{0.2} + 0.021$$
$$G_0 = 0.0936 (tE_{CFS})^{0.417} \tag{3}$$

for tE_{CFS}>38.4 GPa, and

$$s_0 = \frac{3100}{tE_{CFS}} f_c'^{0.2} + 0.034$$
$$G_0 = 1 + \frac{25500}{tE_{CFS}} \tag{4}$$

for tE_{CFS}<38.4 GPa, and:

$$\tau_{max} = 9.1 f_c'^{0.2} tE_{CFS} \times 10^{-5} \le 3.49 f_c'^{0.2} \tag{5}$$

In the above equations f_c' is the concrete compressive strength, τ is the bond stress, τ_{max} is the maximum bond stress; t is the thickness of the CFS and E_{CFS} its stiffness along the fiber direction, s_0 is the slip corresponding to the maximum bond stress, s is the slip, G_0 has the significance of initial shear stiffness of the interface-bonding layer and D^* represents its degradation function defined as:

$$D^* = 1 - \exp\left[\alpha \left(\frac{s}{s_0}\right)^{-\beta}\right]$$
$$\alpha = \ln\left(1 - \frac{1}{G_0}\right) \tag{6}$$
$$\beta = 0.2665 (tE_{CFS})^{0.083} \le 0.64$$

The units used in all equations are mm and MPa.

Using a degradation function derived fro m the Eq. 1 to 6 the shear stiffness is re-evaluated for each sampling point of the interface-bonding element at each loading step according to the magnitude of the maximum slip that was registered at the location of the sampling point during the loading history. Figure 3 presents the shear stiffness degradation and slip relationship for different number of CFS layers derived from the bond stress and slip relationship plotted in Figure 1.

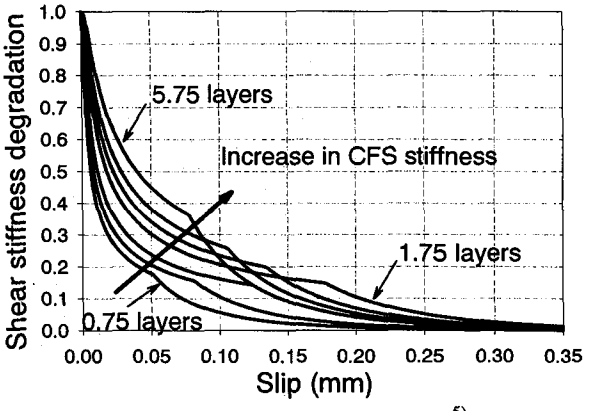

Fig. 3 Shear stiffness degradation[5)]

In order to verify if the FEM program can predict correctly the behaviour of strengthened RC members the results of three tests with unstrengthened and strengthened RC columns subjected to monotonic lateral loading were used.

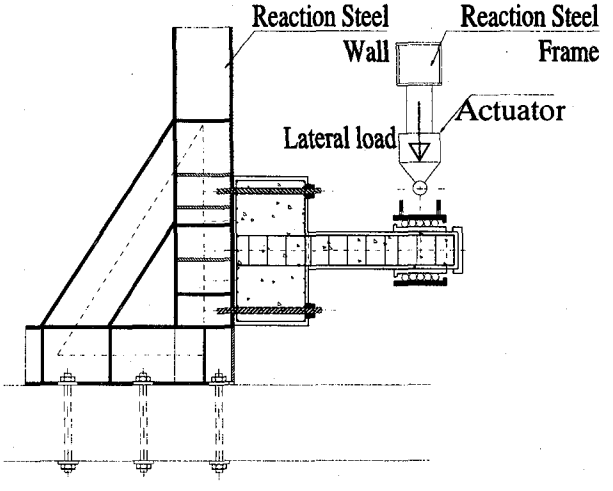

Fig. 4 Test setup

The test specimens have been designed in such way that they fail in shear. For this purpose the equations for shear strength given "Standard Specifications for Design and Construction for Concrete Structures – 1986(Part 1-Design)"[7)] were used. Each specimen was a single prismatic column plus a strong footing ensemble. The column had a rectangular cross-section of 25x25 cm with rounded corners (R=3.5cm), and a total length of 100 cm. All specimens had the same reinforcement detailing. For the strengthened test specimens, the CFS was bonded to the concrete surface and impregnated with epoxy resin. During the tests, displacements of the loading point and strains in the reinforcing bars and CFS were measured in

detail. A rigid steel reaction frame was used to test all specimens. The specimen was connected to this reaction frame by 4 Ø22mm high-strength steel rods, which were prestressed at 294kN each. A ±294kN (±15cm maximum displacement range) actuator was used to apply the lateral load. Figure 4 shows the test setup. Each stirrup that was observed during tests had 6 strain gauges. All data was scanned and recorded immediately after each step in loading. Figures 5 and 6 are showing the position of the strain gauges on CFS stripes for specimens SS2 and SS3 respectively.

The steel reinforcement was five D25 (SD345) for longitudinal reinforcement (symmetric reinforcement), and round bar Ø6 for transverse reinforcement at 15cm spacing. The mechanical properties of the reinforcement are shown in Table 1.

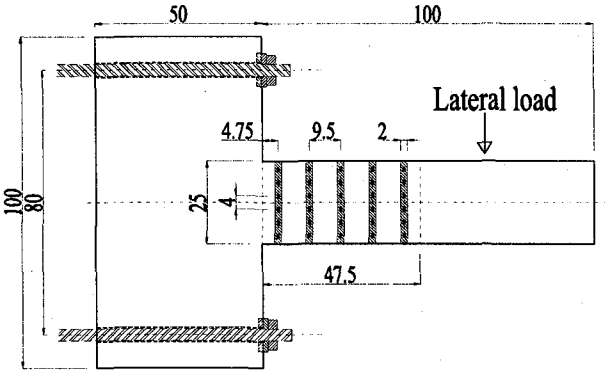

Fig. 5 CFS strain gauges in specimen SS2

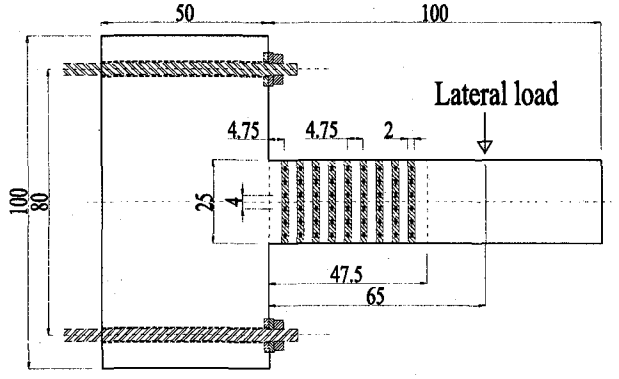

Fig. 6 CFS strain gauges in specimen SS3

Table 1 Mechanical properties of reinforcement

Material	Steel	Steel	CFS
Type	Ø6	D25	FTS-C1-20
Cross-sectional area (cm^2)	0.28	5.07	0.111/10cm width
Young's modulus (GPa)	206	188	230
Yield strength (MPa)	226	382	-
Tensile strength (MPa)	343	N.A.	3480

Table 2 Details of the specimens

Specimen	SS1	SS2	SS3
f'_c (MPa)	25.7	22.7	29.6
Concrete Young's modulus (GPa)	19.0	19.6	21.5
CFS (2cm width)	NO	5 @ 9.50cm	9 @ 4.75cm
Peak value of shear force (kN) experiment	143.1	163.2	193.0
Peak value of shear force (kN) analysis	142.3	169.2	201.1

Nittetsu Composite provided the CFS; the stress-strain relationship of CFS is linear-elastic until fracture. The details of specimens and the concrete strength measured on cylinders immediately after the test for each specimen are given in Table 2.

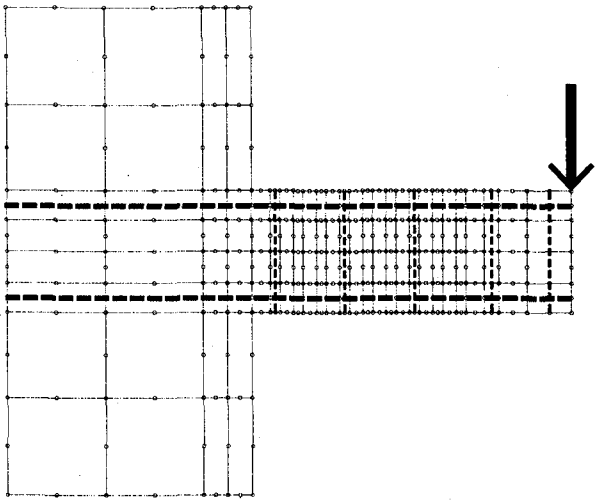

Fig. 7 FEM mesh for specimen SS1

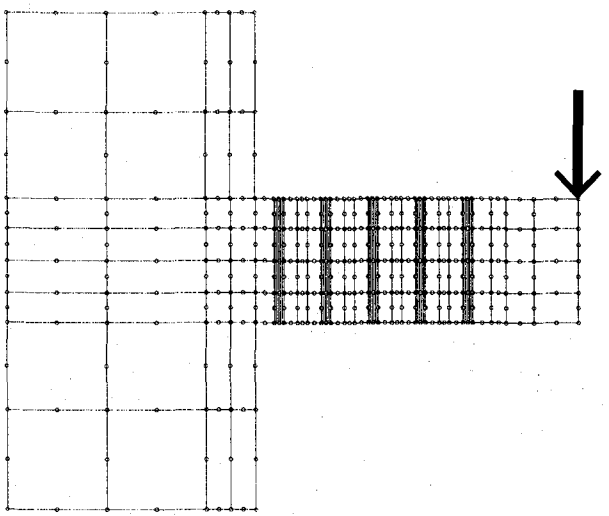

Fig. 8 FEM mesh for specimen SS2

Figures 7, 8 and 9 show the finite element meshes of the specimens analyzed in this study for the specimen without strengthening and strengthened specimens. In Figure 7 the dashed lines indicate the elements with reinforcement (some of the base reinforcement is not represented).

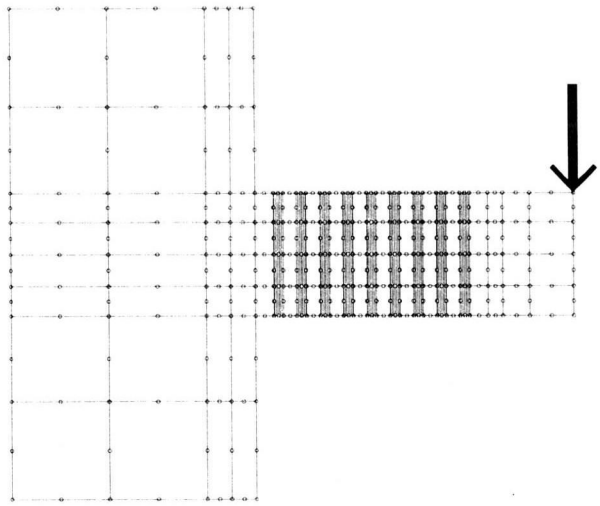

Fig. 9 FEM mesh for specimen SS3

In Figures 8 and 9 the hatched elements indicate the location of the CFS stripes for the case of 5 and 9 stripes respectively (steel reinforcement was not represented). In all cases the base was considered as fixed. In the analysis the enforced displacement is applied at the loading point until peak load was observed.

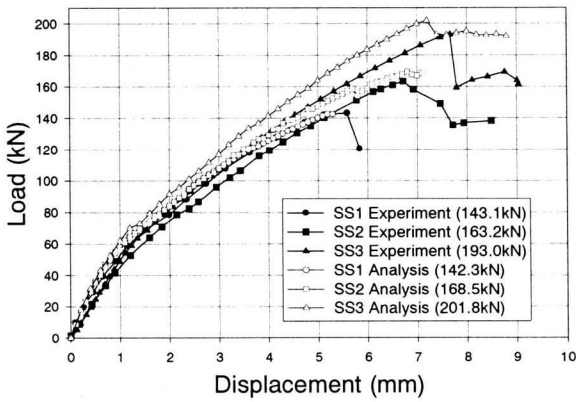

Fig. 10 Load-displacement relationships

Figure 10 presents the plots for load-deflection curves of the specimens considered in this study. The difference between the deflection measured in experiment and the one obtained from FEM analysis is considered to be due to a slip of the column base on the reaction wall, which was not measured during experiment. It can be observed that the analysis results reasonably agree with the experimental observations. The peak load calculated by FEM is shown in Table 2. For the strengthened specimens, SS2 and SS3, there is a difference in the peak load between the experimental and FEM analysis with 3.2% and 4.6% respectively, compared to the experimental one. In both the experiment and analysis fracture of CFS stripe occurred before the peak load in specimen SS2, while no fracture before the peak load in specimen SS3. In experiments, for all specimens tested, at the peak load the crushing of the concrete in the compression zone was observed. After the crushing of the concrete occurred, the resisting force dropped considerably. In the FEM analysis, extensive softening of the concrete in the compression zone was observed in the loading step following the step in which the maximum load was registered. The strengthening effect of the CFS stripes can be clearly observed in both the experimental and analytical results.

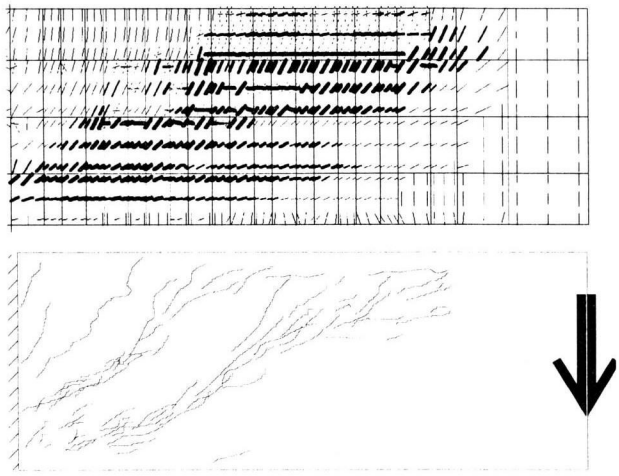

Fig. 11 Crack patterns in FEM analysis and experiment for specimen SS3

Figure 11 shows the crack patterns obtained in the FEM analysis and the one observed in experiment respectively. In the crack pattern obtained by FEM analysis each line represents the information for the area numerically covered by a Gauss point. Because the program uses the smeared crack concept, the represented crack pattern may not coincide geometrically with the one observed in experiment as it was pointed out by An et al[6]. It can be said that there is a good agreement between analysis and experimental observations.

Using the maximum strains in stirrups and CFS stripes recorded along a major shear crack during experiments, the corresponding stresses and shear force components carried by the transverse reinforcement (stirrups) and CFS were calculated. Locations of the maximum strains are indicated in Figure 11. From the FEM program output, the maximum stress in the transverse reinforcement and CFS stripes was used to calculate the same components of the resisting shear force. The shear resisting force by concrete was calculated by subtracting the shear resisting components by transverse reinforcement and CFS stripes from the total shear force.

Figures 12, 13 and 14 show variation of the shear force carried by concrete, steel stirrup and CFS stripe in the experiment and FEM analysis with total shear force. The shear force carried by concrete in the analysis is less than that in the experiment, while the shear force carried by stirrup in the analysis is greater than that in the experiment except at ultimate. The shear force carried by CFS stripe in the analysis is slightly greater than that in the experiment. Although there is some discrepancy, generally the analytical results agree with the experimental ones. Shear force carried by concrete decreases after shear cracking and then increase after yielding of stirrup. In the unstrengthened specimen SS1 the shear force carried by concrete increases linearly until the peak load, while it increases nonlinearly and reach its

peak in the strengthened specimens SS2 and SS3.

The shear force carried by concrete at the peak load in the unstrengthened specimen is greater than that in the strengthened specimens. The shear force carried by stirrup increases steadily after shear cracking and reaches its yielding stage. For the same total shear force the shear force carried by stirrup decreases as the amount of CFS stripes increases.

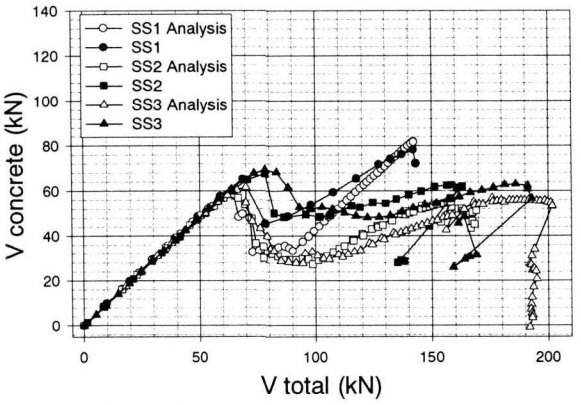

Fig. 12 Shear force carried by concrete

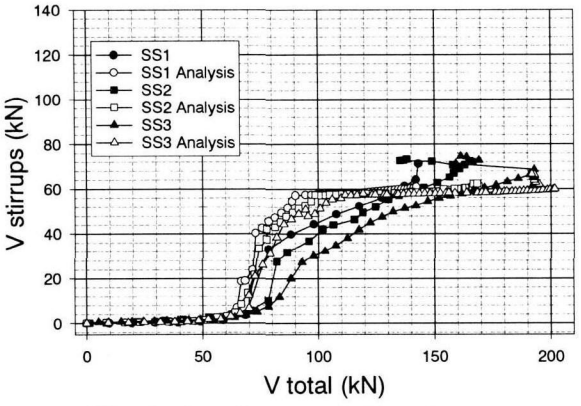

Fig. 13 Shear force carried by stirrups

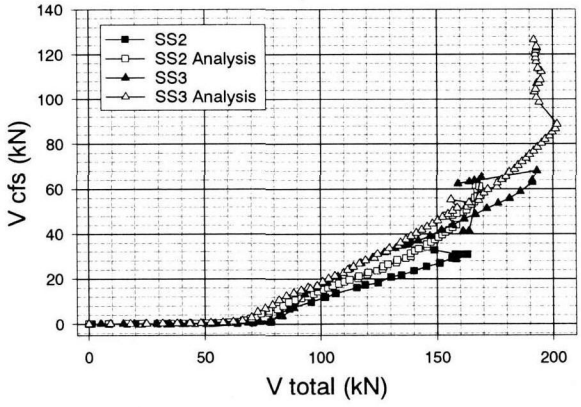

Fig. 14 Shear force carried by CFS stripes

The shear force carried by CFS stripe increases linearly until the first fracture of stripe. The shear force carried by CFS stripe in specimen SS3 is greater than that in specimen SS2 at the peak load and for the same total shear force. Since the shear forces carried by concrete and stirrup in specimens SS2 and SS3 are almost the same at ultimate, the shear force carried by CFS stripe is only the source to increase shear capacity. By comparing unstrengthened and strengthened specimens, the greater shear force by CFS compensates the less shear force carried by concrete and increases shear capacity.

Figure 15 presents the stress in the stirrups for all specimens analysed at the moment when the total resisting force is 140kN. Because at that moment all stirrups have already yielded in diagonal cracking zone (see Fig. 11), it cannot be observed a big difference in the stress magnitude between the three cases. The only difference is that the unstrengthened specimen shows wider areas where the yielding stress value was reached in comparison with the strengthened ones.

Figure 16 indicates the stress along the fiber direction in the CFS stripes for the strengthened specimens. It can be observed that stress in CFS is greater in diagonal cracking zone. The stress in the stripe for specimen SS3 is less than that of the stripe in specimen SS2.

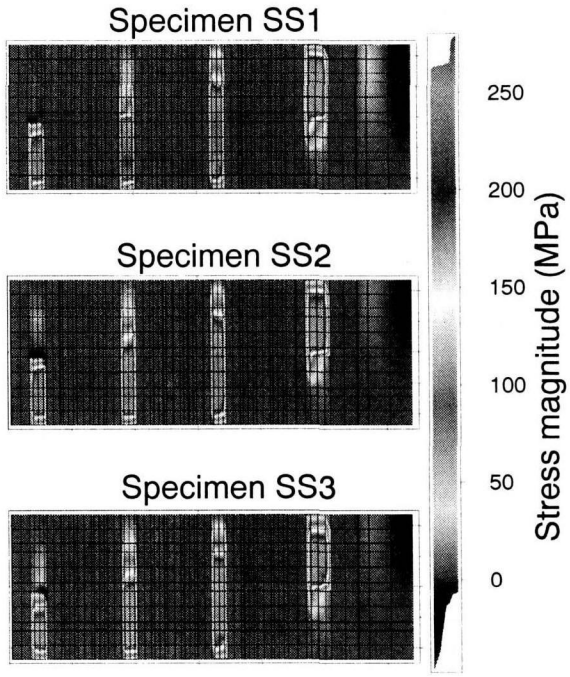

Fig. 15 Stress in the stirrups at 140kN lateral load

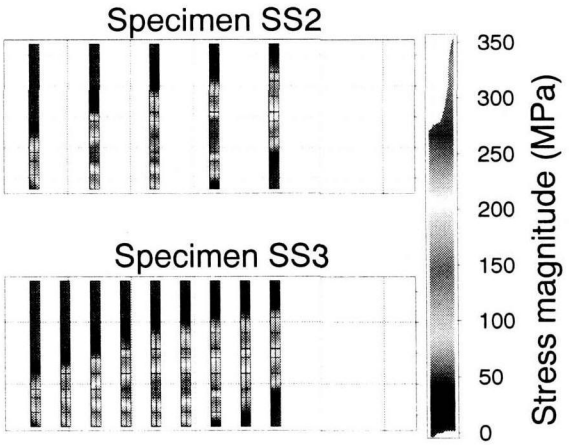

Fig 16 Stress in CFS stripes at 140kN lateral load

Figure 17 presents the bond stress in the interface-bonding layer for the strengthened specimens. The locations marked by circles in Figure 17 indicate the zones where the bond stress is null and complete loss of

bond has already occurred. They also indicate the path where the maximum stresses in stirrups and CFS stripes were observed in the analysis. This path was observed not to change its location during the loading process and selected for calculation of the shear resisting force.

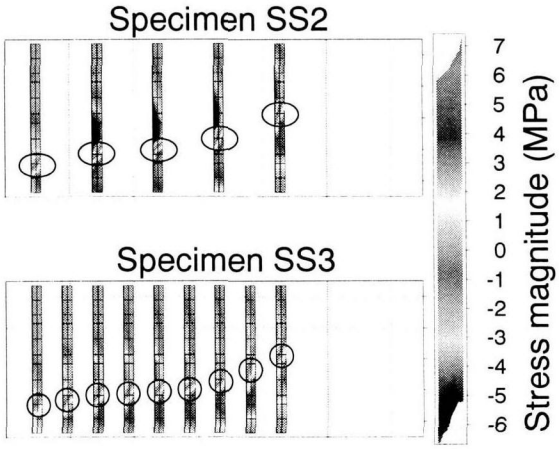

Fig. 14 Bond stress in the interface-bonding layer at 140kN lateral load

By comparing the experimental observations with the FEM analytical results it is concluded that the new elements for CFS and interface-bonding layer implemented by the authors in the original program can simulate correctly the behaviour of the CFS stripes bonded with epoxy resin on RC elements. It is also concluded that the FEM analysis is reliable in predicting the shear strength of RC columns with externally bonded CFS stripes.

3. Model of shear-resisting mechanism

Using the FEM program presented in the previous section four new specimens were investigated using the same FEM meshing. The details of the new specimens are given in Table 3.

Table 3 Details of the specimens

Specimen	SS4	SS5	SS6	SS7
f'$_c$ (MPa)	29.6	29.6	29.6	29.6
Concrete Young's modulus (GPa)	21.5	21.5	21.5	21.5
Stirrups	Ø6 @ 15cm	2×Ø6 @ 15cm	NO	NO
CFS (2cm width)	NO	NO	9 @ 4.75cm	2×9 @ 4.75cm
Peak value of shear force (kN)	146.6	175.7	180.9	191.5

The stirrup's reinforcing ratio for specimen SS5 was two times the one of specimen SS4.

The thickness, t_{CFS} of the CFS stripes for specimens SS6 and SS7 was selected in such a way that at ultimate the CFS stripes should carry the same amount of shear force as the maximum shear force carried by the stirrups of specimens SS4 and SS5 as shown in Eq. (7).

$$t_{CFS} = \frac{A_{web} f_{yweb} / s_{web}}{b_{CFS} f_{CFS} / s_{CFS}} \tag{7}$$

where A_{web} is the area of stirrups; f_{yweb} is the yielding strength for the stirrups; s_{web} is the stirrups spacing; b_{CFS} is the width of the CFS stripes; f_{CFS} is the fracture strength of the CFS stripes; s_{CFS} is the CFS stripes spacing.

For prediction of shear capacity of strengthened column, a shear-resisting model is considered. The shear-resisting model is assumed to be essentially the same as Sato et al's model[1] as follows (see Figure 18):

$$V = V_{cpz} + V_{web} + V_{str} - V_{com} \tag{8}$$

where V_{cpz} is the shear resisting force of concrete at the compression zone, V_{web} is the shear resisting force of the web reinforcement at the shear cracking surface, V_{str} is the shear resisting force given by the other components at the shear cracking surface, V_{com} is the shear resisting force give by the concrete in the horizontal surface linking the compression zone with the cracking surface.

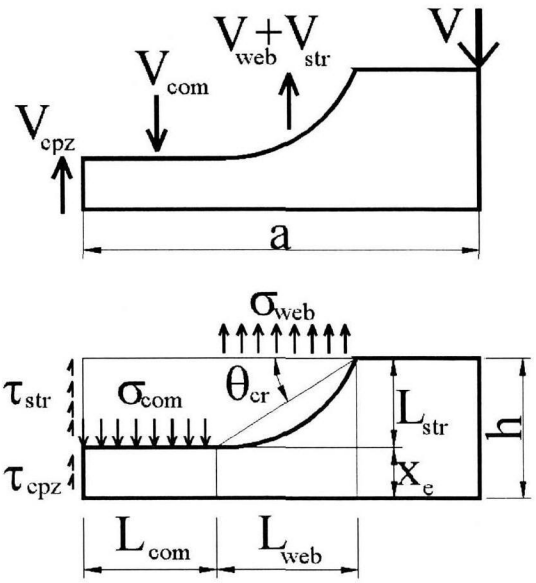

Fig. 18 Shear-resisting model and stresses

Equation 8 can be rewritten as:

$$V = bx_e\tau_{cpz} + p_w bL_{web}\sigma_{web} + bL_{str}\tau_{str} - bL_{com}\sigma_{com} \tag{9}$$

where τ_{cpz} is the average shear stress at the compression zone:

$$\tau_{cpz} = 0.65 f_c' \sin\alpha\cos\alpha \tag{10}$$

$$\alpha = \tan^{-1}\left(\frac{d}{a}\right) \tag{11}$$

σ_{web} is the average tensile stress of web reinforcement at the shear-cracking surface;

$$\sigma_{web} = E_{web}\varepsilon_{web} \tag{12}$$

$$\varepsilon_{web} = 0.0053 \frac{\sqrt{f_c'}}{\sqrt{a/d}+1} e^{-\frac{1000}{p_s E_s} - 0.05\sqrt{p_{web} E_{web}}} \quad (13)$$

τ_{str} is the average shear stress at the shear-cracking surface:

$$\tau_{str} = \sqrt[3]{f_c'} \frac{1.28}{\sqrt{a/d}+1} \quad (14)$$

σ_{com} is the average compressive stress at the horizontal zone:

$$\sigma_{com} = 0.64 f_c' \left(\frac{a}{d}\right)^{-1} \sin^2 \beta \quad \beta = 32^\circ \quad (15)$$

L_{web} is the projection on horizontal of the shear-cracking surface:

$$L_{web} = \frac{L_{str}}{\tan \theta_{cr}} \quad \theta_{cr} = 45^\circ \quad (16)$$

L_{str} is the corresponding vertical projection of the shear-cracking surface:

$$L_{str} = h - x_e \quad (17)$$

L_{com} is the length of the horizontal connecting zone:

$$L_{com} = \frac{a}{h} x_e \quad (18)$$

x_e is the depth of the compression zone:

$$\frac{x_e}{x} = \frac{1 - e^{-\left(\frac{a}{d}\right)}}{1 + 3.2^{-0.12(p_{web} E_{web})^{0.4}}} \quad (19)$$

$$x = -np_s d + \sqrt{(np_s d)^2 + 2np_s d^2} \quad (20)$$

b and h are the RC element width and height, n is the ratio between the longitudinal reinforcement and concrete Young modulus, α and β are the angle of the principal stresses at compression zone and horizontal zone, respectively.

If at the ultimate stage the average tensile strain in the web is grater than the yielding strain of the stirrups, the stirrup strain ε_{web} is calculated substituting E_{web} from Equation (13) with the equivalent Young's modulus for stirrups, E_{eq}[3]. The equivalent modulus is defined as:

$$E_{eq} = f_{yweb} / \varepsilon_{web} \quad (21)$$

where f_{yweb} is the yielding strength of the web reinforcement.

The path to calculate shear force components in the FEM analysis is slightly different from that in this model. This is because in the FEM analysis shear reinforcement was modelled discretely while smeared shear reinforcement is assumed in the shear-resisting model.

Figure 19 presents the load-deflection relationships obtained by means of FEM analysis for the specimens presented in Table 3. All specimens failed in shear. For the specimens that had only CFS stripes as web reinforcement, the calculation stopped after the failure of the first stripe.

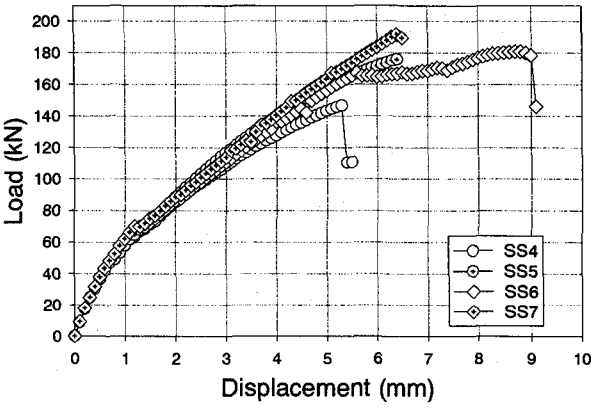

Fig. 19 Load-deflection relationships

Figures 20, 21 and 22 present the components of the total shear resisting force ($V_{concrete}$, $V_{stirrups}$, and V_{CFS} respectively) for specimens SS4, SS5, SS6 and SS7 in order to compare them with those of specimens SS2 and SS3.

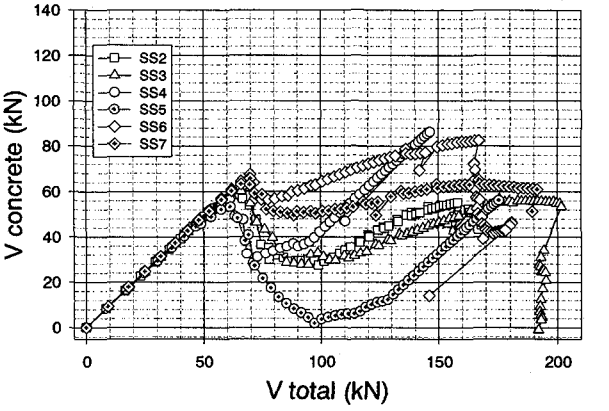

Fig. 20 Shear force carried by concrete

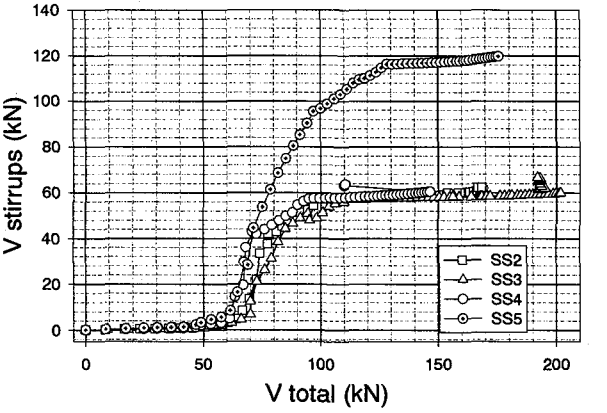

Fig. 21 Shear force carried by stirrups

It can be clearly observed that in the cases where the shear reinforcement is either yielding material (stirrups) or elastic material (CFS stripes) the increase in shear

capacity is caused by the increase of the amount of the shear reinforcement. In addition, each material creates a specific pattern in the development of the component of the resisting shear force carried by the concrete.

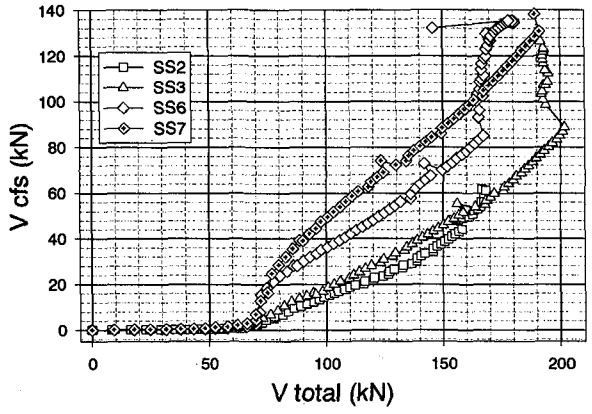

Fig. 22 Shear force carried by CFS stripes

From the results of specimens SS4 and SS5, the shear resisting mechanism of specimens only with stirrups can be seen. The contribution of stirrups at peak load in specimen SS5 is double of that in specimen SS4 since all stirrups have yielded already. The stirrups contribution in specimen SS5 is always greater than that in specimen SS4 for the same total shear force except immediately after shear cracking. The concrete contribution in specimens SS4 and SS5 decreases after shear cracking and increases after the stirrups start to yield. It continues to increase rather linearly until the peak load. Although the concrete contribution in specimen SS5 is less than in specimen SS4 at the peak load, the peak load of specimen SS5 is greater than that of specimen SS4 because of much greater contribution of stirrup.

By comparing the results of specimens SS6 and SS7 where only CFS stripes were used as shear reinforcement, it can be observed that contribution of CFS increases rather linearly after shear cracking until the first fracture of CFS stripe. The total shear force at the first fracture is close to the peak load, although after the first fracture there is a slight increase in total shear force in specimen SS6. If total shear force at the first fracture is considered as shear capacity of the strengthened column, the following can be said: The contribution of CFS in specimen SS7 is greater than that in specimen SS6 at their shear capacity and for the same amount of total shear force. However, the contribution of CFS in specimen SS7 at the shear capacity is not twice as much as that in specimen SS6, although the CFS amount in specimen SS7 is double of that in specimen SS6. The shear force carried by concrete decreases immediately after shear cracking and then increases slightly in specimen SS6 and is almost constant in specimen SS7. After the first fracture of CFS stripe the shear force component of concrete decreases. At the shear capacity of specimen the concrete contribution in specimen SS6 is more than in specimen SS7, however the shear capacity of specimen SS5 is greater than that of specimen SS4 because of greater contribution of CFS.

The cases of specimens SS2 and SS3, where both steel stirrup and CFS stripe were used as shear reinforcement are, compared with cases of specimens SS4 to SS7. Nature of the concrete contribution in specimens SS2 and SS3 is between the case of stirrup alone as shear reinforcement (specimens SS4 and SS5) and the case of CFS alone (specimen SS6 and SS7). The concrete contribution decreases as in specimen SS4 and then increases slightly as in specimen SS6. Nature of stirrup and CFS contributions is essentially the same as the case of specimens SS4 and SS5 and the case of specimens SS6 and SS7. For the same total shear force the stirrup contribution in specimens SS2 and SS3 are smaller than that in specimen SS4 whose stirrup amount is the same as in specimens SS2 and SS3. The same thing can be said for the CFS contribution in specimen SS2 in comparison with specimen SS6 whose CFS amount is almost the same as in specimen SS3.

Table 4 presents the comparison between the values of the average tensile strains of the shear reinforcement obtained using Equation 13 and the ones obtained by from the FEM program.

Table 4 Average tensile strains (μ)

Specimen	SS4	SS5	SS6	SS7
Equation 6	7230	3900	9380	7400
FEM analysis	5010	3470	7660	7350

Although the same FEM program used to develop the model by Sato et al.[1] was used in order to develop the original shear resisting model this study, there is a difference in the way in which the shear reinforcement is described. In this study the shear reinforcement is described in a discrete manner (see Figure 7) while in the original study[1] it was described as spread all over the web. In addition, the boundary conditions and the loading are not exactly same; the original model was developed for beams and in this case we are dealing with columns. This can explain the difference for the cases where the shear reinforcement stiffness is low. The authors of this paper consider that this difference is not so important since the case when both materials are present will always be on the side where the values predicted by Equation 12 agree with the FEM observations.

Based on the finding in the FEM analysis on the shear force components carried by steel stirrup, CFS stripe and concrete in the case where both steel stirrup and CFS stripe are used as shear reinforcement, it is assumed that the stiffness of the shear reinforcement in the shear-resiting model can be taken as the sum of the two components. Then, Equations 13 and 19 should be rewritten as follows:

$$\varepsilon_{web} = 0.0053 \frac{\sqrt{f'_c}}{\sqrt{a/d}+1} e^{\frac{1000}{p_s E_s} - 0.05\sqrt{p_{web}E_{web}+p_{CFS}E_{CFS}}} \quad (22)$$

and

$$\frac{x_e}{x} = \frac{1-e^{-\left(\frac{a}{d}\right)}}{1+3.2^{-0.12(p_{web}E_{web}+p_{CFS}E_{CFS})^{0.4}}} \quad (23)$$

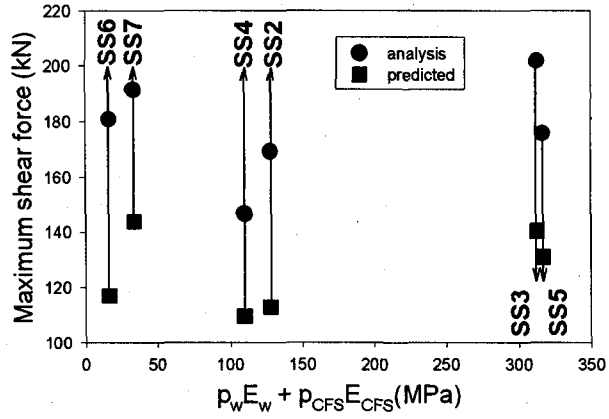

Fig. 23 Comparison between prediction and FEM results

In the case when the average tensile strain is grater than the yielding strain of the stirrups, then the equivalent Young's modulus for stirrups should be used in the above equations. If the average tensile strain is greater even than the fracture strain of the CFS, the value corresponding to the fracture should be considered as upper limitation.

Replacing the Equations 22 and 23 in the calculation procedure, the maximum shear forces have been calculated and they are presented in Figure 23 for comparison with the ones calculated by the FEM analysis.

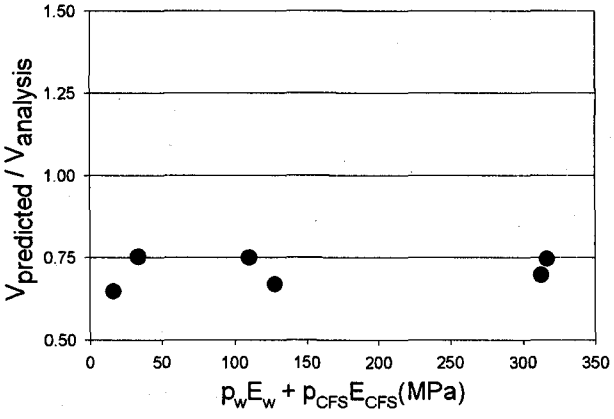

Fig. 24 Shear strength ratio

Figure 24 presents the shear strength ratio for the specimens considered. It is clearly observed that the prediction of the shear capacity of the specimens that have both types of shear reinforcement remains at the same level as the prediction for the specimens with only one type of reinforcement.

It is observed that predictions underestimate the analytical results. The original model for prediction of the shear strength of concrete beams reinforced with FRP rods[3] generally underestimates the shear capacity in the case of low stiffness of the web reinforcement. It could not be explained yet why the predicted value of the shear force for the specimens that have only stirrups is also underestimated in the case of this study. It is believed that the difference between the predicted values and the ones obtained analysis is caused mainly by the difference in the boundary conditions and the way in which the cracking surface is assumed in the original model. Further study to compare the experimental and analytical results with the predicted values should be conducted in order to identify the source of discrepancy.

4. Conclusions

Based on the results presented in this paper it can be concluded that:

1) The FEM program for simulation of the strengthening effect of the CFS composites bonded on the surface of the RC elements was developed. Comparison between experimental and analytical results was presented and it is considered that the FEM analysis offers reliable results on shear resisting mechanism, shear strength and failure mode.
2) Based on the FEM analysis, it was found that shear resisting mechanism of RC member with both steel stirrup and externally-bonded CFS as shear reinforcement is average of that of RC member only with steel stirrup and that of RC member only with externally-bonded CFS.
3) As a result of comparison presented in 2), a modified shear resisting model for RC columns strengthened with externally epoxy-bonded CFS stripes was proposed based on the original shear resisting model of the reinforced and prestressed concrete beams.

From designer's point of view it is practical to use the same equation as for reinforced and prestressed beams in order to calculate the shear strength of the CFS strengthened RC elements by considering the summation of the shear reinforcement stiffness. Still, for the present case, better accuracy is desirable. Therefore, further experimental and analytical study is needed in order to establish how the shear resisting mechanism of RC columns strengthened with CFS is influenced by different parameters, such as: shear span to effective depth ratio, magnitude of axial load, stiffness of reinforcement and concrete compressive strength.

Acknowledgements

This study is a part of the research supported by the Japanese Government (Monbusho) scholarship that is greatly acknowledged. NITTETSU COMPOSITE provided CFS material and epoxy resin.

References

1) Sato, Y., Ueda, T., and Kakuta, Y., "Shear Strength of Reinforced and Prestressed Concrete Beams with Shear Reinforcement", *Concrete Library of JSCE*, NO. 29, pp. 233-247, June 1997.
2) Sato, Y., Ueda, T., and Kakuta, Y., "Shear Strength of Prestressed Concrete Beams with FRP Tendon", *Concrete Library of JSCE*, NO. 27, pp. 189-208, June 1996.

3) Sato, Y., Ueda, T., and Kakuta, Y., "Shear Resisting Model of Reinforced and Prestressed Concrete Beams Based on Finite Element Analysis", *Proceedings of JCI International Workshop on Shear in Concrete Structures*, pp. 159-173, June 1994.
4) Hajime Okamura, Koichi Maekawa, "Nonlinear Analysis and Constitutive Models of Reinforced Concrete", ISBN-7655-1506-0 C 3051, 1991
5) Sirbu, G., Ueda, T., Kakuta, Y., "Finite Element Analysis of Carbon Fiber Sheet Externally Bonded to Concrete", *Journal of Structural Engineering, JSCE*, to be submitted, (2001).
6) An, X., Maekawa, K., Okamura, H., "Numerical Simulation of Size Effect in Shear Strength of RC Beams", *Concrete Library of JSCE*, NO. 31, pp. 323-346, June 1998.
7) Japan Society of Civil Engineers, "Standard Specifications for Design and Construction for Concrete Structures – 1986(Part 1-Design)", 1986.

(Received September 14, 2000)